Theory of disorder-induced acoustic-phonon Raman scattering in quantum wells and superlattices

V. I. Belitsky,* T. Ruf, J. Spitzer, and M. Cardona
Max-Planck-Institut für Festkörperforschung, Heisenbergstrasse 1, D-70569 Stuttgart, Federal Republic of Germany
(Received 19 October 1993)

We present a theory of resonant Raman scattering by acoustic phonons in semiconductor quantum wells and superlattices for the case when translational invariance *along* as well as *perpendicular* to the growth direction is perturbed due to layer thickness fluctuations and interface roughness, both with and without an applied magnetic field. The breakdown of crystal momentum conservation along the growth direction (q_z) leads to scattering from individual layers and folded acoustic phonons from the whole mini-Brillouin zone contribute to a continuous emission background of geminate recombination. The Raman intensity is evaluated from the phonon displacement field. It is proportional to the difference in the amplitudes of pairs of counterpropagating waves constituting each mode. This dependence causes characteristic intensity variations (peaks and dips) superimposed on the emission continuum at energies of gaps of the folded phonon dispersion. Interface roughness also allows for elastic scattering of photoexcited intermediate electronic states in the Raman process into states with nonzero crystal momentum ($q_\parallel$) perpendicular to the growth direction. This momentum can be compensated by acoustic phonons in higher-order Raman processes. Due to this effect internal gaps of the phonon dispersion, e.g., at anticrossings of longitudinal and transverse acoustic branches for $q_\parallel \neq 0$, acquire enough strength to appear in the spectrum as additional structure.

I. INTRODUCTION

Resonant Raman scattering by longitudinal optic (LO) phonons in bulk semiconductors and superlattices has recently been studied intensively. Investigations of the resonant enhancement of the LO Raman intensity due to the quasi-one-dimensional motion of electrons and holes in a high magnetic field and singularities in the density of states for interband magneto-optical transitions between Landau levels have provided information on bulk material parameters, valence band mixing, conduction band nonparabolicity, exciton effects, and electron-phonon interaction.[1–5] Recent theoretical studies of one-LO-phonon Raman scattering for both bulk[2] and quantum well systems[6,7] have focused on the interplay between Landau quantization and electron-phonon interaction via the deformation potential and Fröhlich mechanisms.

For the theoretical description of experimental magneto-Raman profiles, i.e., traces of LO-phonon intensity vs magnetic field for fixed laser excitation energy, the fact that even in the highest presently available steady magnetic fields the cyclotron energy just barely exceeds that of optic phonons poses a formidable problem due to the multitude of terms which contribute significantly to individual interband resonances.[2] To avoid such drawbacks, recent experiments have focused on acoustic-phonon magneto-Raman scattering, especially from folded phonons in superlattices.[8] There it was expected that isolated resonances could be investigated due to the significantly reduced difference between incident and scattered photons. In addition to the characteristic folded phonon doublets, such experiments revealed a continuous Raman emission background in the acoustic-phonon regime which exhibits strongly resonant behavior in a magnetic field.[8–10] Some authors[9] have labeled this emission as *geminate recombination*, thus emphasizing the coherent character of the scattering process, i.e., the fact that one and the same electron-hole pair is excited, scattered, and subsequently recombines. It was suggested that this background is due to Raman scattering by a continuum of acoustic phonons where crystal momentum is not conserved due to quantum well thickness fluctuations and interface roughness.[8,11] Superimposed on the background, characteristic intensity anomalies (peaks and dips) were observed at energies corresponding to gaps of the folded phonon dispersion.[8,11] These peaks and dips have also been noted in earlier studies without magnetic field,[12–15] but no explanation for their relation to the phonon dispersion and to mechanisms for Raman scattering has been given. Qualitatively, the anomalies were attributed to antiresonances associated with acoustic phonons at the mini-Brillouin zone edge,[12] to disorder-induced or q_z nonconserving scattering,[13,14] or to local modes near the dispersion gaps.[8,16] While the observed features of background scattering and peaks and dips are similar for experiments in zero and high magnetic fields, the considerable resonant field enhancement was found indispensable when studying the effects in wider quantum wells, whereas in short-period superlattices signals are strong enough even without field.

In this paper we present a theoretical model of Raman scattering by acoustic phonons in disordered superlattices (SL's) and multiple quantum wells (MQW's) which describes the above features. We treat the intermediate regime where superperiodicity still holds for the phonons

 ©1994 The American Physical Society

but the coherence of electronic states is destroyed by layer thickness fluctuations and interface roughness. In view of the close relation between spectra obtained with and without high magnetic fields, we take advantage of the computationally much easier calculations in the case of Landau quantization. Nevertheless many of the results should apply also without field, a case which, however, can be treated analytically only in a rather simplified approach. After qualitative considerations of the problem in Sec. II, a theoretical model of electron-phonon interaction with acoustic superlattice modes and scattering by interface roughness is presented in Sec. III. From the expressions derived there, the Raman efficiency for isolated quantum well intermediate electronic states is calculated in Sec. IV for both zero and high magnetic fields. In Section V we discuss consequences of the model for the characterization of interface roughness in layered semiconductor structures. Conclusions are given in Sec. VI.

II. QUALITATIVE CONSIDERATIONS

It was shown earlier[8,11,17,18] that the wide background of geminate recombination observed in the acoustic phonon frequency range by backscattering Raman experiments in MQW's and SL's can be explained by a relaxation of crystal momentum conservation along the growth direction. The observation of comparable intensities for "forbidden" background and "allowed" folded phonon peaks in the same spectrum lets us assume that layer thickness fluctuations and interface roughness do not completely destroy superperiodicity but only introduce slight spatial fluctuations of the size-quantized electron and hole energies, both along and perpendicular to the growth direction.

The qualitative picture for the two limits of a perfect multiple quantum well structure and a system strongly disturbed by interface fluctuations can be described in the following way: With good accuracy we can consider electron and hole states to be localized in individual layers and neglect the penetration of their wave functions into the barriers. For a perfect quantum well structure, when all individual layers are exactly the same, the conservation of crystal momentum along the growth direction in a Raman process is due to a summation of contributions from individual wells to the scattering amplitude. Due to Bloch's theorem contributions to the amplitude differ only by exponential factors related to the periodicity of the system. The coherence of individual terms is induced by the photon and phonon waves propagating in the growth direction. In this limit only folded acoustic phonon doublets, i.e., *superlattice features*, would be observed in one-phonon Raman spectra.

In the other limit there are fluctuations in the well widths which result in an energy distribution of size-quantized electron and hole states. For a given laser frequency only some of the wells are in resonance. This reduces the situation to the limit of single quantum well scattering when the scale of the fluctuations is larger than the characteristic *homogeneous broadening* of the electronic states. Individual contributions to the amplitude differ now not only by exponential factors but also by the energy denominators for intermediate electron-hole pair states which are close to zero for wells in resonance with the incident or scattered photons and equal to some energy detuning for others, allowing us to neglect their contribution to the amplitude. Since a random distribution of gaps is expected, we are left with scattering from *single quantum wells* which does not require crystal momentum conservation along the growth direction. This results in the participation in the scattering of acoustic phonons with all wave vectors. The intensity of the background signal decreases with increasing energy detuning. Interface perturbations inherent in real quantum well structures should account for the experimentally observed appearance of single quantum well as well as superlattice features in resonant one-acoustic-phonon Raman scattering.

To understand the occurrence of *anomalies* superimposed on the background near folded phonon dispersion gaps, the dependence of the Raman intensity on phonon crystal momentum has to be considered. In pure one-phonon scattering from a single quantum well, profound dips with zero intensity should be observed at dispersion gaps because of the zero in-plane component of the phonon crystal momentum in backscattering and a vanishing one-dimensional phonon density of states. On the other hand, only the lowest energy Brillouin line and the folded phonon doublets correspond to scattering by the perfect MQW structure with phonons from the folded dispersion. Experimental spectra, however, show a more complicated structure with nonzero intensity inside the gaps and a peculiar sequence of maxima and minima for frequencies near their upper and lower boundaries.[8]

Qualitatively, these variations can be attributed to the symmetries of phonon standing waves at either side of a gap, where displacement profiles in both constituent materials exhibit reflection symmetry with respect to the layers' center planes. Symmetric and anti-symmetric modes are thus related to any gap. These properties are reflected in the Raman intensity and a characteristic alternating sequence of peaks and dips is found, depending on sample parameters. This behavior is analogous to gap oscillations and selection rules for allowed folded phonon doublet scattering near dispersion gaps.[19,20]

Another series of anomalies occurs at energies where longitudinal and transverse acoustic dispersion branches cross. Apparently gaps are also observed at these points, even though the modes should be orthogonal for the (001) propagation direction in which the experiments were performed. In order to explain these features we consider below higher-order Raman processes which involve acoustic phonons and interface roughness. Via such processes scattering by phonons with nonzero values of in-plane crystal momentum becomes possible. Internal gaps of the phonon dispersion where longitudinal and transverse branches do interact may thus contribute to the Raman signal.

III. THEORETICAL MODEL

The interaction of electrons with acoustic phonons can be described by the deformation potential mechanism.[21]

In the following we treat the case of confined quantum well electronic states interacting with folded modes of the acoustic phonon dispersion. Superlattice vibrations are described macroscopically by a periodic variation of densities ρ and elastic constants.[20]

A. Acoustic superlattice phonons

To keep the model general we consider an arbitrary propagation direction for phonons with crystal momentum $\mathbf{q} = (\mathbf{q}_\parallel, q_z)$, i.e., components perpendicular to and along the growth direction ($\mathbf{z}$). The displacement field in unit cell n with two neighboring layers of different materials a and b corresponding to the excitation of a superlattice acoustic phonon can be written as[22]

$$\mathbf{U}_{n\mathbf{q}i}(\mathbf{r}) = C_{i\mathbf{q}} \cdot \exp\left(iq_z^i nd + i\mathbf{q}_\parallel \cdot \mathbf{r}_\parallel\right)\left[\sum_{j=1}^{6} \mathbf{e}_{\mathbf{q}j}^{ai} A_j^i(\mathbf{q}) e^{ik_{zj}^{ai}(\mathbf{q})z}\Theta\left(\frac{a}{2}+z\right)\Theta\left(\frac{a}{2}-z\right)\right.$$
$$\left. + \sum_{j=1}^{6} \mathbf{e}_{\mathbf{q}j}^{bi} B_j^i(\mathbf{q}) e^{ik_{zj}^{bi}(\mathbf{q})(z-\frac{d}{2})}\Theta\left(z-\frac{a}{2}\right)\Theta\left(b+\frac{a}{2}-z\right)\right]. \quad (1)$$

Here $C_{i\mathbf{q}} = \frac{1}{L^{3/2}}\left(\frac{\hbar}{2\rho\omega_{qi}}\right)^{1/2}$, L^3 is the normalization volume, and $\mathbf{e}_{\mathbf{q}j}^{ai,bi}$ is the polarization vector in layers a and b related to the superlattice phonon with wave vector $\mathbf{q}$ from branch i. $A_j^i(\mathbf{q})$ and $B_j^i(\mathbf{q})$ are the amplitudes of the six waves propagating in the a and b layers (i.e., three pairs of counterpropagating waves), respectively. $\Theta(z)$ is a step function which guarantees the value of z being from the interval $(-a/2, +a/2)$ for layer a and ranging within $(a/2, b+a/2)$ for layer b. The superlattice period is $d = a+b$. While $\mathbf{q}$ is the wave vector of the superlattice phonon dispersion, the values of $k_{zj}^{ai,bi}(\mathbf{q})$ are determined by the bulk phonon dispersion relations of the constituent materials. For arbitrary propagation directions they are determined by the Christoffel equation which describes sound propagation in anisotropic media:[22,23]

$$(C_{jlmn}^{a,b} k_l^{ai,bi} k_n^{ai,bi} - \rho_{a,b}\omega_{\mathbf{q}i}^2 \delta_{jm}) e_m^{ai,bi} = 0. \quad (2)$$

C_{jlmn} is the elastic-constant tensor of each layer. The dispersion of phonon frequency $\omega_{\mathbf{q}i}$ as a function of superlattice wave vector $\mathbf{q}$ is found from the system of equations satisfying boundary conditions for the continuity of displacement and stress fields normal to each interface as well as periodicity.[22] In practice, fixed values of ω and $\mathbf{q}_\parallel$ are chosen, the $k_{zj}^{ai,bi}(\mathbf{q})$ are determined from the secular equation

$$\det\left(C_{jlmn}^{a,b} k_l^{ai,bi} k_n^{ai,bi} - \rho_{a,b}\omega_{\mathbf{q}i}^2 \delta_{jm}\right) = 0, \quad (3)$$

and boundary conditions are applied. Note that $\mathbf{k}_\parallel$ and $\mathbf{q}_\parallel$ are identical and must be conserved across each interface, while q_z^i, related to the superperiodic modulation, and the $k_z^{ai,bi}(\mathbf{q})$, corresponding to the z component of the wave vector in the layers, are different. For propagation along the growth direction one obtains six orthogonal modes, one longitudinal acoustic (LA) phonon and two transverse (TA) branches for each of the directions $\pm q_z$ of crystal momentum. By expressing the displacement field as a linear combination of these six modes, the ansatz of Eq. (1) includes the possible conversion of phonons by intermode Bragg reflection when $\mathbf{q}_\parallel \neq 0$. This leads to the appearance of internal dispersion gaps at points other than the mini-Brillouin zone edge or center and causes anticrossings of interacting acoustic phonon branches.[24] Acoustic-phonon transmission spectroscopy and imaging have recently been used for detailed theoretical and experimental studies of these phenomena.[22,25]

B. Electron-phonon interaction

The electron-phonon interaction Hamiltonian for deformation potential coupling is given by the product of a deformation potential constant tensor Ξ^{ij} and the strain tensor

$$\epsilon_{ij}^n(\mathbf{r}) = \frac{1}{2}\left(\frac{\partial U_i(\mathbf{r})}{\partial r_j} + \frac{\partial U_j(\mathbf{r})}{\partial r_i}\right) \quad (4)$$

associated with a phonon mode displacement field $\mathbf{U}_{n\mathbf{q}}(\mathbf{r})$ as given by Eq. (1).[21] i and j are coordinate indices x, y, and z. From Eq. (1) we obtain $\epsilon_{lm}^{n(\mathbf{q}i)}$ in the period n of the superlattice phonon $(\mathbf{q}, i)$ as

$$\epsilon_{lm}^{n(\mathbf{q}i)}(\mathbf{r}) = \epsilon_{lm}^{na(\mathbf{q}i)}(\mathbf{r}) + \epsilon_{lm}^{nb(\mathbf{q}i)}(\mathbf{r})$$
$$= C_{i\mathbf{q}}\frac{i}{2}\exp\left(i\mathbf{q}_\parallel\mathbf{r}_\parallel + iq_z^i nd\right)$$
$$\times\left[\Theta\left(\frac{a}{2}+z\right)\Theta\left(\frac{a}{2}-z\right)\sum_{j=1}^{6}[e_{\mathbf{q}j}^{lai} p_{jm}^{ai}(\mathbf{q}) + e_{\mathbf{q}j}^{mai} p_{jl}^{ai}(\mathbf{q})]\cdot A_j^i(\mathbf{q}) e^{ik_{zj}^{ai}(\mathbf{q})z}\right.$$
$$\left. + \Theta\left(z-\frac{a}{2}\right)\Theta\left(b+\frac{a}{2}-z\right)\sum_{j=1}^{6}[e_{\mathbf{q}j}^{lbi} p_{jm}^{bi}(\mathbf{q}) + e_{\mathbf{q}j}^{mbi} p_{jl}^{bi}(\mathbf{q})]\cdot B_j^i(\mathbf{q}) e^{ik_{zj}^{bi}(\mathbf{q})(z-\frac{d}{2})}\right] \quad (5)$$

with the following notation:

$$p_{jx} = q_x, \quad p_{jy} = q_y, \quad p_{jz}^{ai,bi} = k_{jz}^{ai,bi}(\mathbf{q}). \tag{6}$$

The electron-phonon interaction Hamiltonian is then

$$\begin{aligned}\varphi_{\mathbf{qi}}^{n}(\mathbf{r}) &= \Xi_a^{lm}\epsilon_{lm}^{na(\mathbf{qi})}(\mathbf{r}) + \Xi_b^{lm}\epsilon_{lm}^{nb(\mathbf{qi})}(\mathbf{r}) \\ &= iC_{i\mathbf{q}}\exp\left(i\mathbf{q}_{\|}\cdot\mathbf{r}_{\|} + iq_z^i nd\right) \\ &\quad\times\left[\Theta\left(\frac{a}{2}+z\right)\Theta\left(\frac{a}{2}-z\right)\sum_{j=1}^{6} p_j^{ai}\Xi_{j\mathbf{q}}^{ai}A_j^i(\mathbf{q})e^{ik_{zj}^{ai}(\mathbf{q})z}\right. \\ &\quad\left.+\Theta\left(z-\frac{d}{2}\right)\Theta\left(b+\frac{a}{2}-z\right)\sum_{j=1}^{6} p_j^{bi}\Xi_{j\mathbf{q}}^{bi}B_j^i(\mathbf{q})e^{ik_{zj}^{bi}(\mathbf{q})(z-\frac{d}{2})}\right]\end{aligned} \tag{7}$$

with an effective interaction constant given by

$$\Xi_{j\mathbf{q}}^{ai,bi} = \frac{1}{2}\,\Xi_{a,b}^{lm}[e_{\mathbf{q}j}^{lai,bi}Q_{jm}^{ai,bi}(\mathbf{q}) + e_{\mathbf{q}j}^{mai,bi}Q_{jl}^{ai,bi}(\mathbf{q})], \tag{8}$$

and $\mathbf{Q}_j^{ai,bi} \equiv \mathbf{p}_j^{ai,bi}/p_j^{ai,bi}$, $p_j^{ai,bi} = |\mathbf{p}_j^{ai,bi}|$.

The value of $\Xi_{j\mathbf{q}}^{ai,bi}$ depends on the propagation direction and the polarization of vibrations in the superlattice. For propagation along the growth direction, LA modes have a strain component ϵ_{zz} which yields a nonvanishing contribution to the interaction, while TA modes are orthogonally polarized to $\mathbf{q}$ and do not interact. For crystal momentum $\mathbf{q}_{\|} \neq 0$ the modes are of mixed character and other elements of ϵ, especially ϵ_{xx} and ϵ_{yy}, also contribute. In bulk III-V semiconductors such as GaAs, the longitudinal acoustic deformation potential constant of conduction electrons is much larger than that of valence band states (either longitudinal or transverse).[26,27] It is therefore sufficient to take into account only the pure hydrostatic component of the strain caused by the phonon displacement, i.e., the term transforming like $\epsilon_{xx} + \epsilon_{yy} + \epsilon_{zz}$.[28]

In the following we consider resonant Raman scattering with incident photon frequencies in resonance with electronic transitions in the well material (a layers). Electronic excitations created in the wells may interact with acoustic phonons via the deformation potential. They can also be scattered by the potential due to well width fluctuations and interface roughness. Under these assumptions only that part of the interaction potential which corresponds to the a layer needs to be considered. For a quantum well with z coordinate within $(-a/2, +a/2)$ the electron-phonon interaction potential thus reads

$$\varphi_{i\mathbf{q}}(\mathbf{r}) = iC_{i\mathbf{q}}e^{i\mathbf{q}_{\|}\cdot\mathbf{r}_{\|}}\sum_{j=1}^{6}\Xi_{jq}^{i}p_j^i A_j^i(\mathbf{q})e^{ik_{zj}^i(\mathbf{q})z}, \tag{9}$$

where the index a has been omitted.

C. Interface roughness scattering

Growth imperfections in real semiconductor structures cause the interface between two different materials not to be atomically and electronically flat. We assume imperfections to be randomly distributed along the interfaces in the form of growth islands, where one material penetrates into the adjacent one as a monolayer step of a certain lateral extent.[29,30] This causes local variations in the confinement energies from which electronic states can be scattered with a change of their in-plane crystal momentum component $q_{\|}$.

The interaction potential of electrons or holes with such islands can be written in the following form:

$$\psi(\mathbf{r}_{\|}) = \frac{(2\pi)^2}{L_x L_y}\sum_{\mathbf{q}_{\|}}\chi(\mathbf{q}_{\|})\exp\left[i\mathbf{q}_{\|}\cdot(\mathbf{r}_{\|} - \mathbf{r}_{0\|})\right]. \tag{10}$$

This describes an impuritylike potential with strength $\chi(\mathbf{q}_{\|})$ being constant inside the well along the growth direction and centered at the position $\mathbf{r}_{0\|}$ in the plane. We treat it in the following as a source of scattering for electrons or holes localized in the well assuming averaging over position $\mathbf{r}_{0\|}$ which recovers translational invariance for the in-plane direction.

The physical information on the imperfection of the interface is contained in the Fourier coefficients $\chi(\mathbf{q}_{\|})$. A constant value of χ up to a certain maximum value of $q_{\|}$ ($q_{\|,\max}$) and $\chi = 0$ beyond describes a potential of the type $\sin(q_{\|,\max}r_{\|})/(q_{\|,\max}r_{\|})$. From the first zeros of this potential a characteristic length scale can be derived and interpreted as the size of growth islands. Assuming a Gaussian form of the interface roughness potential for the in-plane direction $\psi(\mathbf{r}_{\|}) \sim \exp(-r_{\|}^2/t^2)$ the Fourier coefficients to be substituted in Eq. (10) are $\chi(\mathbf{q}_{\|}) \sim t^2\exp(-q_{\|}^2t^2/4)$, where t is a characteristic width of the potential.

IV. RAMAN EFFICIENCY

Within a general approach for the Raman intensity[31,32] the scattering efficiency can be written as

$$\frac{d^2S}{d\Omega d\omega_s} = \frac{\omega_s^3\omega_l}{c^4}\frac{n(\omega_s)}{n(\omega_l)}e_{s\alpha}^* e_{s\beta}e_{l\gamma}e_{l\lambda}^*\mathbf{S}_{\alpha\gamma\beta\lambda}, \tag{11}$$

where Ω is the solid angle, c the velocity of light in vacuum, $n(\omega)$ the refractive index, $\mathbf{e}_l(\mathbf{e}_s)$ the polarization vector, $\omega_l(\omega_s)$ the frequency for incident (scattered) radiation, and $\mathbf{S}_{\alpha\gamma\beta\lambda}$ the light scattering tensor of fourth

rank. The diagram technique for calculating $\mathbf{S}_{\alpha\gamma\beta\lambda}$ has been developed in Refs. 31 and 32. In the following we shall evaluate the scattering efficiency for the two experimentally relevant cases of isolated confined electronic states in the presence of and without a strong magnetic field.

A. Raman efficiency in a magnetic field

Figure 1 displays two diagrams for the second order process of an electron being scattered by a superlattice acoustic phonon (wavy lines) and interacting with the interface roughness potential (dash-dotted lines) in a strong magnetic field. For electron and hole states completely confined in the well the numbers of size quantized levels N in optical transitions should be the same. Although in principle there is no N conservation in the vertices of electron-phonon and electron-roughness interaction it was assumed for the diagrams in Fig. 1 since it leads to stronger resonant conditions. The same arguments hold for Landau numbers n. The values of the y component of the wave vector are conserved in all vertices. Conservation of the x component for the phonon crystal momentum and the Fourier harmonic of the interface roughness potential is introduced by the sum over k_y. There is no conservation for the z component of the wave vector for scattering from a single quantum well which is assumed to be dominant because of energy level variations originating from layer thickness fluctuations and interface roughness. Note that the phonons are not affected by the magnetic field, which only leads to an additional confinement of electronic states and, consequently, to an increase of the Raman intensity.[1]

In order to calculate the Raman efficiency we need to evaluate matrix elements with electron and hole wave functions in the well in a high magnetic field. In the Landau gauge they are given by

$$\Psi_{n,N,k_y}(\mathbf{r}) = \frac{\exp(ik_y y)}{\sqrt{L_y}} u_n(x - x_{k_y})\eta_N(z)v_0(\mathbf{r}), \quad (12)$$

where $L_x L_y$ is the area of a quantum well. N and n are quantum numbers of the size-quantized and Landau levels. The wave function of a one-dimensional oscillator

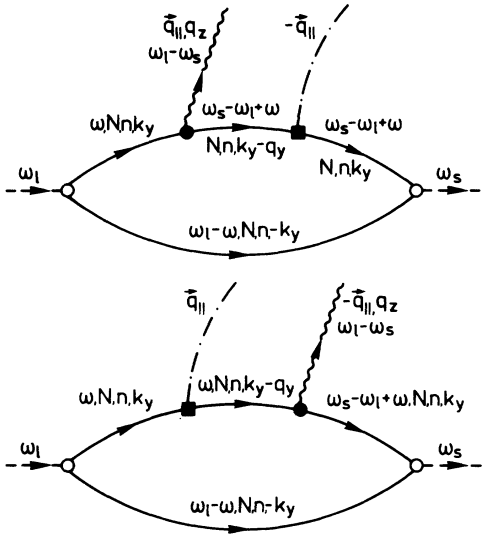

FIG. 1. Diagrams of second-order Raman processes with acoustic-phonon (circle, wavy line) and interface-roughness induced (square, dash-dotted line) scattering of intermediate electronic states.

in the Landau sublevel n is given by

$$u_n(x) = \left(\frac{m_e\omega_e}{\pi\hbar}\right)^{1/4} \frac{1}{\sqrt{n}} \exp\left(-\frac{m_e\omega_e}{2\hbar}x^2\right) \times H_n\left(x\sqrt{\frac{2m_e\omega_e}{\hbar}}\right), \quad (13)$$

with the Hermite polynomials $H_n(x)$ and $\omega_{e(h)} = eH/m_{e(h)}c$ being the cyclotron frequency for electrons and holes of mass $m_{e(h)}$. The wave functions for electron and hole states in the well are

$$\eta_N(z) = \sqrt{\frac{2}{a}}\cos\frac{\pi N z}{a}, \quad N = 1,3,5,\ldots \quad (14)$$

$$\eta_N(z) = \sqrt{\frac{2}{a}}\sin\frac{\pi N z}{a}, \quad N = 2,4,6,\ldots . \quad (15)$$

The center position of the oscillator for electrons and holes is equal to $x_{k_y} = \mp l_H^2 k_y$, $l_H = \sqrt{\hbar c/eH}$ is the magnetic length and $v_0(\mathbf{r})$ the Bloch function. After integration over the z coordinate within the well and over $\mathbf{r}_{\|}$, the matrix element for the interaction of Eq. (9) and the wave functions of Eq. (12) reads

$$R^i_{nN}(k_y,\mathbf{q}) = \langle N,n,k_y'|\varphi_{i\mathbf{q}}(\mathbf{r})|N,n,k_y\rangle = iC_{i\mathbf{q}}\delta_{k_y,k_y'+q_y}\sqrt{N_{i\mathbf{q}}+1}\sum_{j=1}^{6}\Xi^i_{j\mathbf{q}}p^i_j A^i_j(\mathbf{q})\exp\left[\pm il_H^2 q_x\left(k_y-\frac{q_y}{2}\right)\right]K_n(q_{\|})\Upsilon_N[k^i_{zj}(\mathbf{q})], \quad (16)$$

$$K_n(q_{\|}) = \exp\left(-\frac{l_H^2 q_{\|}^2}{4}\right)L_n\left(\frac{l_H^2 q_{\|}^2}{2}\right), \quad (17)$$

$$\Upsilon_N(k_z) = \frac{\sin\left(\frac{ak_z}{2}\right)}{\frac{ak_z}{2}}\frac{4N^2}{4N^2-\left(\frac{ak_z}{\pi}\right)^2}, \quad (18)$$

where $L_n(x)$ is the Laguerre polynomial and $N_{i\mathbf{q}}$ the Bose-Einstein distribution. Under resonant conditions and strong magnetic quantization it suffices to consider only the electron-hole pair states with specific quantum numbers N and n which are closest to the incoming or outgoing resonance considered.

In the same way we find for the matrix element of electron and hole interaction with the interface roughness potential

$$T_n(\mathbf{q}_\parallel) = \langle N, n, k_y' | \psi_{\mathbf{q}_\parallel}(\mathbf{r}_\parallel) | N, n, k_y \rangle = \frac{(2\pi)^2}{\sqrt{L_x L_y}} \delta_{k_y, k_y' + q_y} \chi(\mathbf{q}_\parallel) \sqrt{n_d} \times \exp\left[\pm i l_H^2 q_x \left(k_y - \frac{q_y}{2}\right)\right] K_n(q_\parallel), \quad (19)$$

where n_d is the areal concentration of defects related to the interface roughness.

An important feature of the matrix element for interaction with phonons is the appearance of a factor which involves amplitudes $A_j^i(\mathbf{q})$ of all six waves in the layer and results in a strong dependence of the Raman efficiency on the relative contribution of the pairs of waves which propagate in opposite directions with respect to the growth direction.

With the help of Eqs. (11), (16), and (19) we find finally for the differential efficiency of scattering corresponding to the contribution of the two diagrams shown in Fig. 1 for a Raman shift $\omega_l - \omega_s$

$$\frac{dS}{d\omega_s} = S_0 J \left(N_{\omega_l - \omega_s} + 1\right) \times \frac{[2\Omega_{nN} - (\omega_l - \omega_s)]^2 + 4\Gamma^2}{\left(\Omega_{nN}^2 + \Gamma^2\right)^2 \{[\Omega_{nN} - (\omega_l - \omega_s)]^2 + \Gamma^2\}^2}, \quad (20)$$

where

$$S_0 = \frac{\omega_s}{\omega_l} \frac{n_s}{n_l} |\mathbf{e}_l \cdot \mathbf{p}_{cv}|^2 |\mathbf{e}_s \cdot \mathbf{p}_{cv}|^2 \frac{e^4 n_d}{m_0^4 c^4 \hbar^5 \rho (\omega_l - \omega_s) L_z l_H^4}, \quad (21)$$

$$\Omega_{nN} = \omega_l - \omega_g - \omega_N^e - \omega_N^h - (n + 1/2)(\omega_e + \omega_h), \quad (22)$$

$$J = \sum_i \int dq_\parallel \, K_n^4(q_\parallel) W_i(\mathbf{q}) \delta(\omega_l - \omega_s - \omega_{\mathbf{q}i}), \quad (23)$$

and

$$W_i(\mathbf{q}) = \left| \sum_{j=1}^{6} \Xi_{j\mathbf{q}}^i p_j^i A_j^i(\mathbf{q}) \Upsilon_N[k_{zj}^i(\mathbf{q})] \chi(\mathbf{q}_\parallel) \right|^2. \quad (24)$$

The contributions of electrons and holes to the homogeneous broadening are included in $\Gamma = (\gamma_e + \gamma_h)/2$. Ω_{nN} measures the detuning of the exciting laser photons from the interband critical point at which resonance occurs. Its energy is given by the contributions of the gap and the confinement and cyclotron energies for electrons and holes. The appearance of L_z in the denominator of Eq. (21) results from the calculation of the scattering efficiency for a single quantum well when the superlattice vibrations were normalized to the sample size L_z. The total efficiency of scattering is independent of the normalization volume. The diagrams in Figs. 1(a) and 1(b) result in similar contributions to the scattering efficiency with slightly different energy denominators. Due to the elastic character of interface roughness scattering, the first diagram in Fig. 1 gives the main contribution to scattering in incoming resonance whereas the second one is mainly important for outgoing resonance. This follows from the second power to which the resonant term related to the electron-hole pair state before and after the interaction with interface roughness occurs in the energy denominator for the scattering efficiency.

B. Raman efficiency without magnetic field

The case of zero magnetic field can be treated in a way similar to scattering in the presence of a strongly quantising magnetic field but taking all intermediate states of the electronic subsystem as plane waves in the lateral directions instead of the wave functions of Eqs. (12) and (14). The spectrum of phonon excitations as well as the electron-phonon and electron-roughness interaction [Eqs. (9) and (10), respectively] can be taken in the same form as for the case of a high magnetic field.

Calculations without magnetic field become more cumbersome because of the additional integral over $q_\parallel$ of the electronic intermediate states. This integration cannot be performed analytically without some approximations such as, for example, assuming an infinite effective mass for holes.[34] Below we neglect $q_\parallel$ in the energy denominators corresponding to the electron Green's functions (see diagrams in Fig. 1). Since in our model all features related to folded acoustic-phonon dispersion gaps reflect the properties of the matrix elements for electron-phonon and electron-roughness interaction rather than those of resonant denominators, we believe that such an approximation is valid. Making use of Eqs. (9)–(11), (18), (19), (21), (23), and (24) we find

$$\frac{dS}{d\omega_s} = \frac{\tilde{S}_0 \tilde{J} (N_{\omega_l - \omega_s} + 1)}{(\Omega_N^2 + \Gamma^2) \{[\Omega_N - (\omega_l - \omega_s)]^2 + \Gamma^2\}}, \quad (25)$$

where

$$\tilde{J} = \sum_i \int dq_\parallel \, W_i(\mathbf{q}) \delta(\omega_l - \omega_s - \omega_{\mathbf{q}i}), \quad (26)$$

$\Omega_N = \omega_l - \omega_g - \omega_N^e - \omega_N^h$, and $\tilde{S}_0 = S_0(\mu^2 l_H^4/\hbar^2)$. Because of the approximation taken, the resonance behavior of Eq. (25) is more singular than it would be if $q_\parallel$ was taken into account in the energies of intermediate electronic states. It is known that in the two-dimensional case resonances have logarithmic character.[33,34] By comparison of Eqs. (20) and (25) we find that the crucial dependence on $\mathbf{q}$, which is responsible for the intensity

anomalies superimposed on the continuum emission, follows from the dependence of the scattering efficiency on $W_i(\mathbf{q})$. This function is involved in the equations for both Raman scattering in zero and in high magnetic fields.

V. DISCUSSION

In the following we shall illustrate consequences of our model of acoustic-phonon Raman scattering in disordered multiple quantum wells and superlattices.

Among the phonons with crystal momentum along the growth direction, only the longitudinal acoustic modes have a strain component ϵ_{zz} which allows for diagonal matrix elements of the deformation potential interaction with the confined electronic states. The TA modes may couple light hole with heavy hole bands but do not lead to backscattering. Therefore Eq. (9) reduces to the sum over the two LA modes with superlattice crystal momentum $\pm q_z$. Each of these modes is a linear combination of two counterpropagating LA waves with wave vectors $\pm k_z$ in the well layers. For brevity their amplitude factors are labeled by $A_\pm$, respectively. The electron-phonon Hamiltonian of Eq. (9) thus reduces to

$$\phi_{i\mathbf{q}}(\mathbf{r}) = iC_{i\mathbf{q}} e^{i\mathbf{q}_\parallel \mathbf{r}_\parallel} \Xi k_z \left(A_+ e^{ik_z z} - A_- e^{-ik_z z}\right). \quad (27)$$

Evaluating the matrix elements with electron wave functions from Eqs. (14) and (15) the Raman efficiency is found proportional to

$$\frac{dS}{d\omega_s} \sim |A_+ - A_-|^2. \quad (28)$$

It is via this term that the folded character (i.e., the Bragg reflections) of the phonon dispersion enters into the Raman spectrum. Otherwise the result for $q_\parallel = 0$ is analogous to the one derived in Ref. 8. Figure 2 shows (a) the LA phonon dispersion, (b) the variation of the above intensity factor vs Raman shift, and (c) the experimental Raman spectrum for a symmetric GaAs-AlAs superlattice with layer thicknesses of 16 monolayers.[8] The spectrum was measured at 6 K in a magnetic field of 11 T using the $\bar{z}(\sigma^-,\sigma^-)z$ scattering geometry. The excitation energy was 1.727 eV, in resonance with the $n = 1$ Landau level of the lowest heavy hole to electron transition. At the energies of dispersion gaps in Fig. 2(a) Bragg reflection at the interfaces causes the LA phonons to have a displacement field of standing waves, i.e., the amplitudes $A_\pm$ are equal in magnitude but either opposite or equal in their relative signs. Consequently the Raman intensity factor in Fig. 2(b) vanishes at one side of each gap whereas it has a finite value on the other one. This behavior is reflected in Fig. 2(c) for all intensity anomalies related to LA dispersion gaps. To obtain the experimentally observed spectrum, the Raman efficiency has to be evaluated according to Eq. (20), which yields a continuously decreasing background of geminate recombination with superimposed peaks and dips due to the intensity factor. Further comparisons between experiment and theory will be published elsewhere. We want to emphasize once more that the key point of our model

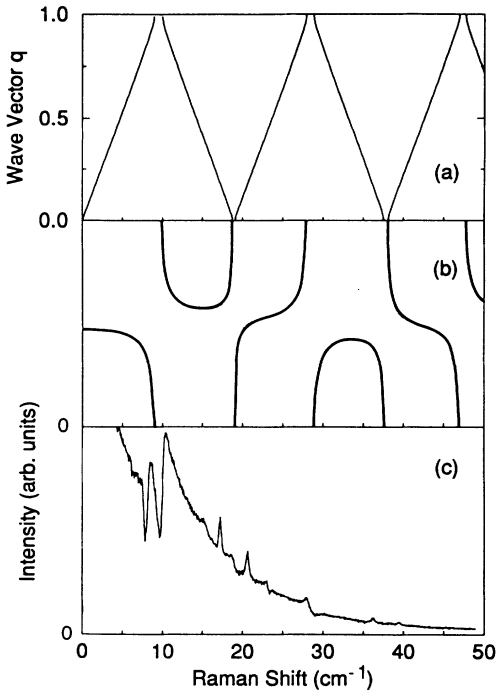

FIG. 2. (a) LA phonon dispersion for a symmetric GaAs-AlAs superlattice with layer thicknesses of 16 monolayers; (b) Raman intensity factor according to Eq. (28); (c) experimental Raman spectrum for such a structure showing peaks and dips superimposed on a continuous emission background.

is the interplay between electronic disorder, leading to q_z nonconserving scattering, and superlattice effects, which persist for the phonons and are manifested by the intensity factor of Eq. (28).

As mentioned in Sec. II, the behavior of the Raman intensity near boundaries of the mini-Brillouin zone is analogous to gap oscillations studied earlier.[19,20] According to Fig. 3.8 of Ref. 20 or Fig. 2 of Ref. 19 the magnitudes of folded phonon dispersion gaps oscillate in a characteristic fashion as a function of relative layer thicknesses. This causes Raman-active zone boundary modes to lie either below or above the nonactive ones in energy. Changes in this relative ordering occur each time the magnitude of a gap goes through zero. Figure 3 illustrates the variations of the intensity factor for LA phonons in GaAs-AlAs superlattices with a constant period of 30 monolayers. The various curves were calculated for different thickness ratios α of AlAs layers with respect to the total period. The respective values of α are given next to each trace. While the magnitude of the gap widens for the first zone edge anomaly near 10 cm^{-1} for values of α around 0.5, the characteristic vanishing of the intensity at the lower side of the gap and the overshoot at the higher energy does not change over the whole range of α. This reflects the behavior found in Ref. 20 where the lowest energy gap does not go through zero for any value of α, except for those corresponding to bulk materials. For the first zone center feature near 20 cm^{-1} the symmetric and antisymmetric modes change their relative positions only

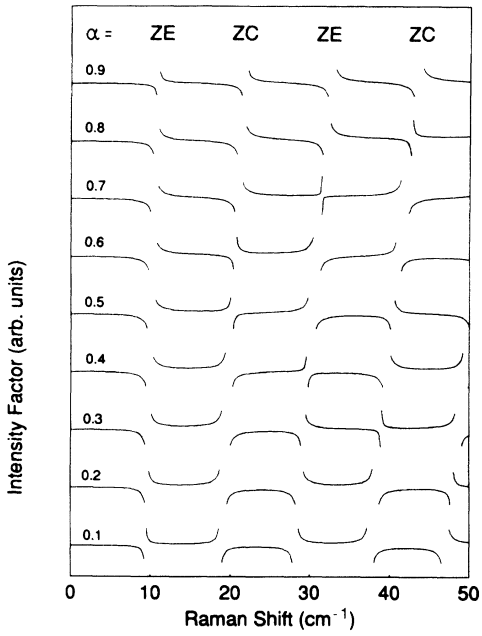

FIG. 3. Raman intensity factor according to Eq. (28) for a GaAs-AlAs superlattice with period of 30 monolayers and varying relative thicknesses. The ratio α of barrier layer to total thickness is given for each curve.

once near $\alpha = 0.55$, the point where that gap vanishes.[20] The two remaining anomalies involve two and three flips, respectively, corresponding to zero gaps at $\alpha \simeq 0.4$ and 0.7 and $\alpha \simeq 0.3$, 0.55, and 0.8.

In Secs. III and IV we demonstrated how superlattice phonons with $q_{\|} \neq 0$ may contribute to backscattering Raman spectra via a second-order mechanism involving one step mediated by the interface-roughness potential. Due to the dependence of the Raman intensity on crystal momentum, internal gaps may also cause intensity anomalies in the spectra. Structures of this origin are shown in Fig. 4. Figure 4(a) shows the experimental Raman spectrum of the (16/16)-monolayer GaAs-AlAs MQW structure discussed before. It is to be compared with the best fit from our model, shown in Fig. 4(b). In Fig. 4(b) an integration over $q_{\|}$ was performed up to a maximum value of $q_{\|} = 0.4\pi/d$. To approximate the interface-roughness potential, Fourier coefficients $\chi(\mathbf{q}_{\|})$ were chosen constant up to that value of $q_{\|}$ and zero beyond. The features marked by asterisks are anomalies due to gaps of the LA-phonon dispersion at the edge and center of the mini-Brillouin zone. They have the characteristic vanishing and enhanced scattering intensities predicted by the factor from Eq. (28) and Fig. 2(b). The anomalies marked with triangles originate in internal gaps where LA and TA dispersions couple and anticross. Intensity anomalies predicted for these gaps are also in close agreement with the experiment. The one TA branch which couples to LA phonons near the first gap at the Brillouin zone edge acquires enough strength to show up in the spectrum as a kink labelled with the circle in Fig. 4(b). The inclusion of phonons with $q_{\|} \neq 0$ in the calculation leads to a change in the phonon density of states from one-dimensional to a modified three-dimensional character. Consequently the Raman intensity in Fig. 4(b) vanishes for shifts approaching zero. Presumably due to insufficient stray light rejection, this decrease in the intensity could not be observed for the present sample. Clear indications of the expected behavior, however, have been seen in other short-period superlattices.[11] A comparison of the observed anomalies with LA and TA phonon dispersions is given in Fig. 4(c). The interacting quasilongitudinal and qua-

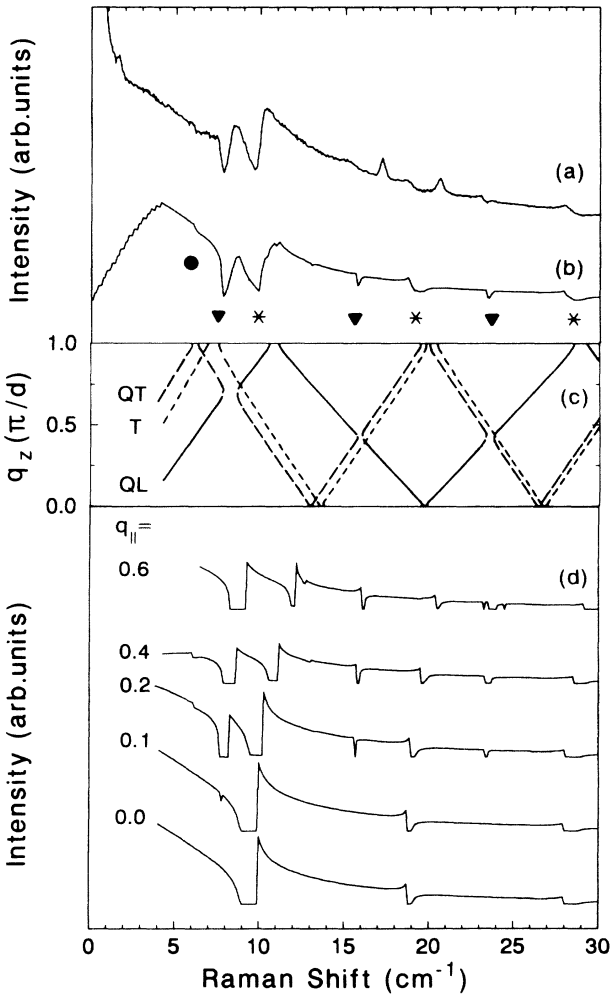

FIG. 4. (a) Experimental Raman spectrum of the (16/16) monolayer GaAs-AlAs superlattice compared to (b) the best theoretical profile obtained by integration over a range of in-plane crystal momenta $q_{\|}$. Stars, triangles, and the circle denote peaks and dips due to LA, LA-TA internal, and TA dispersion gaps, respectively. (c) Exemplary folded phonon dispersion vs q_z calculated for a nonzero in-plane wave vector $q_{\|} = 0.4\pi/d$. Solid, long-dashed, and short-dashed lines indicate the dispersion branches of quasilongitudinal (QL), quasitransverse (QT), and pure transverse (T) modes. Zone-edge and internal gaps give rise to the intensity anomalies denoted in (b). (d) Theoretical spectra calculated for various values of $q_{\|}$ indicated next to each trace in units of π/d. See text for details on parameters used in both calculations and experiment.

sitransverse modes are given by solid and long-dashed lines, respectively. The dispersions have been calculated with an in-plane crystal momentum component of $q_{\|} = 0.4\pi/d$. Zone edge and internal dispersion gaps can be directly compared to the respective background intensity anomalies of Figs. 4(a) and 4(b). The purely transverse acoustic branch (T), given by the short-dashed lines in Fig. 4(c), causes neither continuum emission nor anomalies.

Figure 4(d) shows a number of spectra calculated for different values of $q_{\|}$ given next to each trace in units of π/d. Parameters were chosen according to the experimental conditions under which the spectrum in Fig. 4(a) was obtained. The homogeneous broadening Γ was taken to be 1 meV. For $q_{\|} = 0$ only the three anomalies of the LA dispersion are obtained. As $q_{\|}$ increases, LA-TA anticrossing features and the kink at the TA zone edge gap develop signatures of increasing strength. Increasing $q_{\|}$ also shifts the dispersion gaps towards higher energies. From this sequence it becomes evident that by comparison with experimental spectra a range of values for $q_{\|}$ can be determined. For $q_{\|}$ around zero, the LA-TA features are much less pronounced than for larger in-plane wave vectors. On the other hand, for $q_{\|}$ too large, such as illustrated by the top curve of Fig. 4(d), absolute and relative energies of peaks and dips deviate increasingly from their experimental positions. We find that by integration over a range of $q_{\|}$ the ratio of the LA anomaly to the LA-TA anticrossing and the TA kink can be adjusted quite sensitively. The spectrum in Fig. 4(b) was thus obtained for $0 \leq q_{\|} \leq 0.4\pi/d$, assuming constant $\chi(q_{\|}) \neq 0$ within and a zero value outside of this range.

As mentioned in Sec. III the Fourier spectrum chosen corresponds to approximating the roughness potential by islands of the form $\sin(q_{\|,\max} r_{\|})/(q_{\|,\max} r_{\|})$. From the first zeros of this expression, a characteristic length scale can be determined. For the sample investigated a value of $\lambda \simeq 450$ Å is obtained. The height of roughness-potential steps has been recently determined from variations of hole-intersubband energies due to inhomogeneous broadening in electronic Raman scattering experiments from p-modulation doped GaAs-$Al_{0.43}Ga_{0.57}As$ MQW and was found to be of the order of a monolayer fluctuation.[30] However, no information on the lateral extension of these defects could be obtained. Due to their sensitivity to $q_{\|}$, Raman spectra in the acoustic-phonon regime allow the characterization of the extension and possibly the size distribution of growth islands in epitaxially grown interfaces.

We want to point out that the expression for the Raman efficiency in the presence of a strong magnetic field given by Eqs. (20)–(24) contains a factor $K_n(q_{\|})$ [Eq. (17)], which leads to an exponential suppression of the scattering intensity for in-plane crystal momenta $q_{\|}$ larger than the inverse of the magnetic length l_H. In the treatment for zero magnetic field this factor, which comes from the overlap of Landau wave functions, does not appear. Experimental spectra, measured both with and without magnetic fields, show similar behavior for the LA zone edge and LA-TA internal gap features from which lateral length scales of interface roughness were obtained. The main effect of the magnetic field is that it provides additional confinement and thus an enhancement of the Raman intensity which is especially important for wider quantum wells. In short-period superlattices, however, the effects can be studied even without field.[16] The differences in the two limits of our model are likely to be reconciled by a more involved treatment which takes excitonic effects into account.

The spectra shown in Figs. 4(b) and 4(c) contain no folded phonon doublets. This is due to the single quantum well scattering treated in our model. To include crystal momentum-conserving contributions, a coherent summation over several inhomogeneously broadened MQW has to be performed. The ratio of folded-phonon doublet to background-emission intensity has recently been analyzed with respect to the relative magnitude of homogeneous and inhomogeneous broadenings of MQW electronic structure.[18]

VI. CONCLUSIONS

We have developed a theoretical model of acoustic phonon Raman scattering which explains the continuous emission background and superimposed peaks and dips in geminate recombination spectra of semiconductor multiple quantum wells and superlattices. Disorder from layer thickness fluctuations and interface roughness causes an inhomogeneous broadening of electronic structure. Individual confined levels within this distribution can be resonantly excited in a Raman experiment so that translational invariance and crystal momentum selection rules break down for the electronic states, whereas the vibrational structure remains rather unaffected. This leads to scattering from all phonon modes of the reduced mini-Brillouin zone. Gaps of the folded phonon dispersion appear as characteristic peaks and dips in the spectra. Their intensities follow from the dependence of the Raman efficiency on phonon crystal momentum. Second-order Raman processes with one step mediated by interface-roughness scattering have been invoked to explain the observation of intensity anomalies at internal anticrossing gaps of LA and TA dispersions. The ratio of LA zone edge and LA-TA internal gap features depends on the lateral extension of the roughness potential. This provides a possibility to determine characteristic sizes of growth islands.

ACKNOWLEDGMENTS

V.I.B. thanks the Max-Planck-Gesellschaft for financial support and the Max-Planck-Institut für Festkörperforschung for hospitality. Thanks are due to M. P. Chamberlain for discussions and a critical reading of the manuscript.

* On leave from the A. F. Ioffe Physical-Technical Institute, Russian Academy of Science, 194021 St. Petersburg, Russia.

[1] V. I. Belitsky, A. V. Goltsev, I. G. Lang, and S. T. Pavlov, Zh. Eksp. Teor. Fiz. **86**, 272 (1984) [Sov. Phys. JETP **59**, 155 (1984)].

[2] C. Trallero-Giner, T. Ruf, and M. Cardona, Phys. Rev. B **41**, 3028 (1990).

[3] T. Ruf, R. T. Phillips, A. Cantarero, G. Ambrazevičius, M. Cardona, J. Schmitz, and U. Rößler, Phys. Rev. B **39**, 13 378 (1989).

[4] T. Ruf, R. T. Phillips, C. Trallero-Giner, and M. Cardona, Phys. Rev. B **41**, 3039 (1990).

[5] T. Ruf and M. Cardona, Phys. Rev. B **41**, 10 747 (1990).

[6] A. Cros, A. Cantarero, C. Trallero-Giner, and M. Cardona, Phys. Rev. B **45**, 6106 (1992).

[7] A. Cros, A. Cantarero, C. Trallero-Giner, and M. Cardona, Phys. Rev. B **46**, 12 627 (1992).

[8] V. F. Sapega, V. I. Belitsky, T. Ruf, H. D. Fuchs, M. Cardona, and K. Ploog, Phys. Rev. B **46**, 16 005 (1992).

[9] P. S. Kop'ev, D. N. Mirlin, V. F. Sapega, and A. A. Sirenko, Pis'ma Zh. Eksp. Teor. Fiz. **51**, 624 (1990) [JETP Lett. **51**, 708 (1990)].

[10] D. N. Mirlin, I. A. Merkulov, V. I. Perel', I. I. Reshina, and A. A. Sirenko, Solid State Commun. **82**, 305 (1992).

[11] T. Ruf, V. I. Belitsky, J. Spitzer, V. F. Sapega, M. Cardona, and K. Ploog, Phys. Rev. Lett. **71**, 3035 (1993).

[12] C. Colvard, T. A. Gant, M. V. Klein, R. Merlin, R. Fischer, H. Morkoç, and A. C. Gossard, Phys. Rev. B **31**, 2080 (1985).

[13] J. Sapriel, J. Chavignon, F. Alexandre, and R. Azoulay, Phys. Rev. B **34**, 7118 (1986).

[14] A. B. Talochkin, V. A. Markov, I. G. Neizvestnyĭ, O. P. Pchelyakov, M. P. Sinyukov, and S. I. Stenin, Pis'ma Zh. Eksp. Teor. Fiz. **50**, 21 (1989) [JETP Lett. **50**, 24 (1989)].

[15] D. J. Mowbray (private communication); F. Calle, D. J. Mowbray, D. W. Niles, M. Cardona, J. M. Calleja, and K. Ploog, Phys. Rev. B **43**, 9152 (1991).

[16] T. Ruf, V. F. Sapega, J. Spitzer, V. I. Belitsky, M. Cardona, and K. Ploog, in *Phonons in Semiconductor Nanostructures*, Vol. 236 of *NATO Advanced Study Institute, Series E: Applied Sciences*, edited by J. P. Leburton *et al.* (Kluwer, Dordrecht, 1993), p. 83.

[17] V. F. Sapega, V. I. Belitsky, A. J. Shields, T. Ruf, M. Cardona, and K. Ploog, Solid State Commun. **84**, 1039 (1992).

[18] D. N. Mirlin, I. A. Merkulov, V. I. Perel', I. I. Reshina, A. A. Sirenko, and R. Planel, Solid State Commun. **84**, 1093 (1992).

[19] P. V. Santos, L. Ley, J. Mebert, and O. Koblinger, Phys. Rev. B **36**, 4858 (1987).

[20] B. Jusserand and M. Cardona, in *Light Scattering in Solids V*, edited by M. Cardona and G. Güntherodt, Topics in Applied Physics Vol. 66 (Springer, Heidelberg, 1989), p. 49.

[21] A. Pinczuk and E. Burstein, in *Light Scattering in Solids I*, edited by M. Cardona, Topics in Applied Physics Vol. 8 (Springer, Heidelberg, 1983), p. 23.

[22] S. Tamura, D. C. Hurley, and J. P. Wolfe, Phys. Rev. B **38**, 1427(1988); S. Tamura and J. P. Wolfe, *ibid.* **35**, 2528 (1987).

[23] B. A. Auld, in *Acoustic Fields and Waves in Solids* (Wiley, New York, 1973), Vol. 1, p. 210.

[24] F. Calle, M. Cardona, E. Richter, and D. Strauch, Solid State Commun. **72**, 1153 (1989).

[25] D. C. Hurley, S. Tamura, J. P. Wolfe, and H. Morkoç, Phys. Rev. Lett. **58**, 2446 (1987).

[26] M. Cardona and N. E. Christensen, Phys. Rev. B **35**, 6182 (1987).

[27] D. D. Nolte, W. Walkiewicz, and E. E. Haller, Phys. Rev. Lett. **59**, 501 (1987).

[28] H.-R. Trebin, U. Rössler, and R. Ranvaud, Phys. Rev. B **20**, 686 (1979).

[29] M. A. Herman, D. Bimberg, and J. Christen, J. Appl. Phys. **70**, R1 (1991).

[30] P. Ils, J. Kraus, G. Schaack, G. Weimann, and W. Schlapp, J. Appl. Phys. **70**, 5587 (1991).

[31] E. L. Ivchenko, I. G. Lang, and S. T. Pavlov, Fiz. Tverd. Tela (Leningrad) **19**, 2751 (1977) [Sov. Phys. Solid State **19**, 1610 (1977)]; Phys. Status Solidi B **85**, 51 (1978).

[32] A. V. Goltsev, I. G. Lang, S. T. Pavlov, and M. F. Bryzhina, J. Phys. C **16**, 4221 (1983).

[33] W. Kauschke, N. Mestres, and M. Cardona, Phys. Rev. B **36**, 7469 (1987).

[34] L. I. Korovin, S. T. Pavlov, and B. É. Éshpulatov, Zh. Eksp. Teor. Fiz. **99**, 1619 (1991) [Sov. Phys. JETP **72**, 904 (1991)].